Supplementary Information:
Metamaterial fibres for sub-diffraction imaging and focusing at terahertz frequencies over optically long distances

Alessandro Tuniz[1], Korbinian J. Kaltenecker[2,3,4], Bernd M. Fischer[2,3], Markus Walther[2,4], Simon C. Fleming[1], Alexander Argyros[1] and Boris T. Kuhlmey[1,5*]

[1] Institute of Photonics and Optical Science (IPOS), School of Physics, The University of Sydney, NSW 2006 Australia

[2] Freiburg Materials Research Center, University of Freiburg, Stefan-Meier-Strasse 21, D-79104 Freiburg, Germany

[3] French-German research institute of Saint-Louis, 5, rue du Général Cassagnou, 68301 Saint-Louis, France

[4] Institute for Physics, University of Freiburg, Hermann-Herder-Strasse 3, D-79104 Freiburg, Germany

[5] Centre for Ultrahigh bandwidth Devices for Optical Systems (CUDOS), The University of Sydney, New South Wales 2006, Australia

* boris.kuhlmey@sydney.edu.au

Supplementary Figures

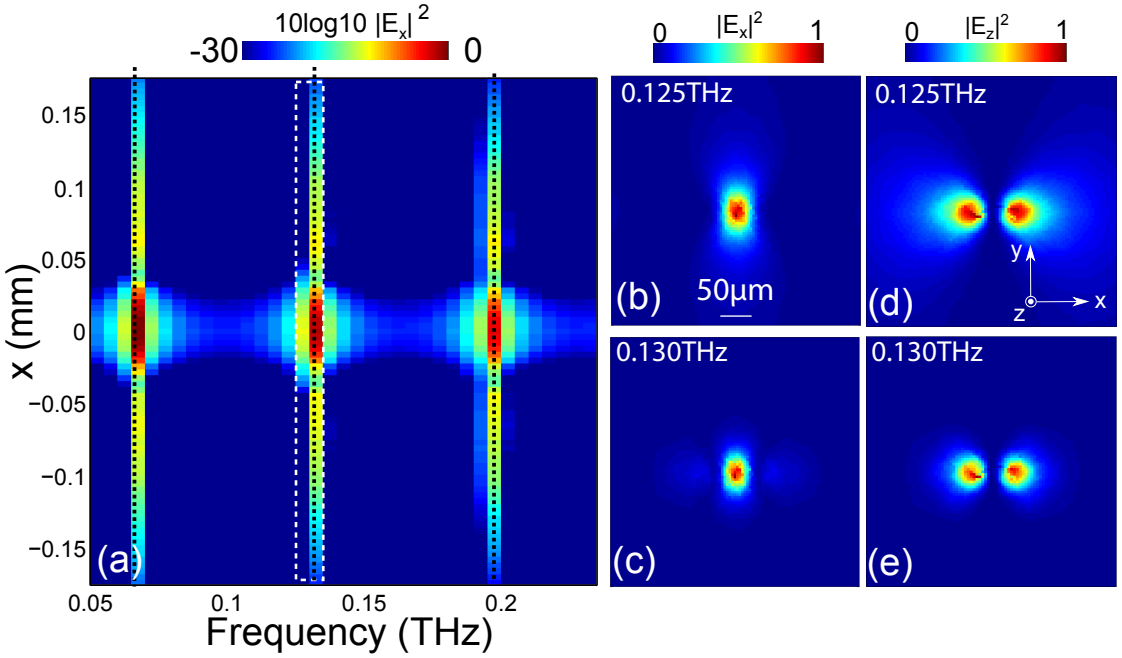

Supplementary Figure S 1: Example of point spread function. To characterize the imaging properties of the straight fibre device, an example point spread function (PSF) is calculated using a finite element solver. We model a slab of Zeonex containing 12×13 hexagonally-arranged 20 μm indium wires, with 50 μm centre-to-centre pitch, and appropriate material electromagnetic parameters accounted for[29,31]. To minimize computational times for the frequency sweep, we consider a slab length of 1.5 mm, and include periodic boundary conditions to model an infinite array in x and y. A point dipole current in the x-direction is placed between wires on the surface of the slab. The field at the output of the slab allows one to obtain the point spread function. (a) Simulated frequency-dependent point spread function in terms of x-polarized field intensity at $y = 0$ with 5 GHz resolution, as a function of x and frequency. Fields are taken 30 μm from the output facet to minimize meshing artefacts arising from the boundaries. The intensity is plotted on a logarithmic colour scale, normalized to the maximum of the entire window, rather than to the maximum at each frequency used in other figures. This highlights the resonant behaviour of the hyperbolic slab: note the Fabry-Perot (FP) resonant transmission (black dotted lines show the predicted resonances with 66 GHz free spectral range), where overall intensity is maximum. (b)-(c) Spatial intensity of the x-polarized field at the output of the slab for two significant cases around the second Fabry-Perot resonance region, as highlighted by the white dashed rectangle in (a). The PSF just below the FP resonance in (c) shows sidelobes 10 dB below the cental lobe that are absent in (b); however the central lobe itself is narrower for (b) with FWHM along x $\text{FWHM}_x = 32\,\mu$m and along y $\text{FWHM}_y = 54\,\mu$m versus $\text{FWHM}_x = 38\,\mu$m and $\text{FHWM}_y = 75\,\mu$m for (c). (d)-(e) Spatial intensity of the z-polarized field at the output of the slab for two significant cases around the second Fabry-Perot resonance region. Note the presence of two lobes here is consistent with the field patterns of a dipole source in the x direction. The PSF is narrowest at 0.130 THz, where each lobe possesses $\text{FWHM}_x = 37\,\mu$m and $\text{FWHM}_y = 44\,\mu$m, with a considerably reduced spread in the y direction as expected from the homogenized model for which the z-field only emerges from the extraordinary waves. In contrast, at 0.125 THz each lobe possesses $\text{FWHM}_x = 100\,\mu$m and $\text{FWHM}_y = 52\,\mu$m.

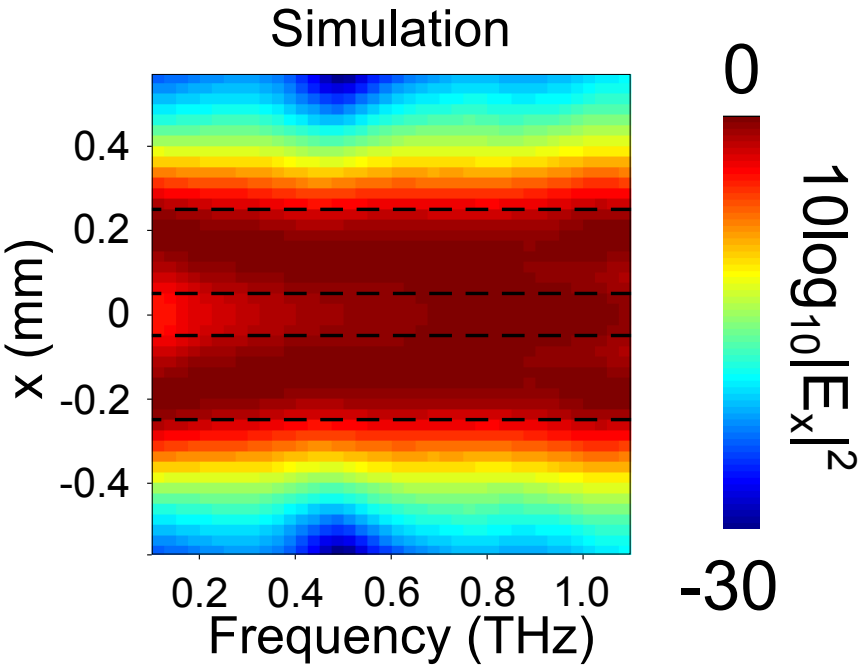

Supplementary Figure S 2: Bare 200 μm apertures separated by 100 μm - simulation. Simulated frequency-dependent beam profile, for two 200 μm apertures separated by 100 μm at 125 μm distance from the apertures, reproducing the observed features of the experiment [Fig. 2(d)]. The dashed lines indicate the location of the apertures.

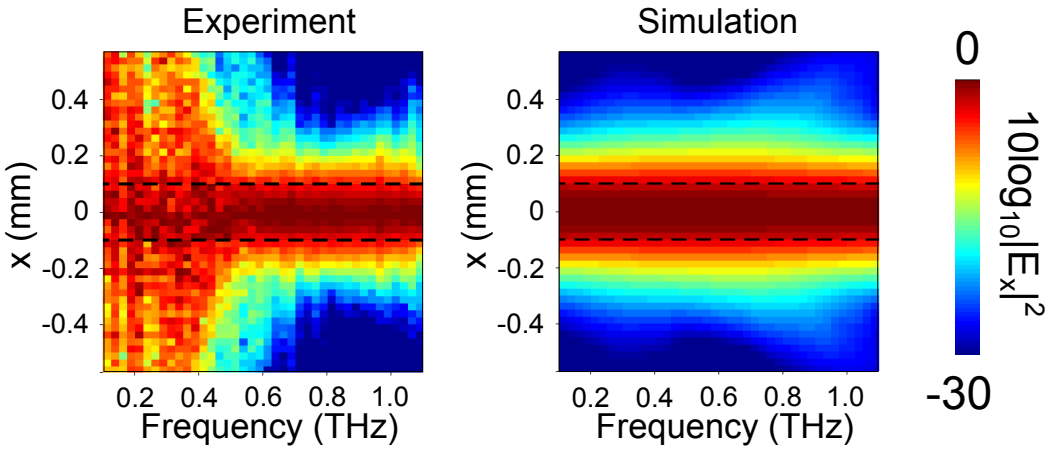

(a) (b)

Supplementary Figure S 3: Bare 200 μm aperture - experiment and simulation. (a) Experimental and (b) simulated frequency-dependent beam profile for the single aperture, as a function of x and frequency. The simulation considers fields at a distance of 75 μm from the disc along x at $y = 0$, whereas the experiment is averaged over $y = 0 \pm 100\,\mu$m. The dashed lines indicate the location of the aperture. A comparison with the image of a single 200 μm aperture in contact with a metamaterial fibre of 3.4 mm length [Fig. 2(l)] shows that the 200 μm hole is well-resolved at most frequencies. At frequencies below 0.5 THz, the image is much noisier, a consequence of the high-pass filtering behaviour of the sub-wavelength aperture,[32] but the aperture can still be resolved. Note at these frequencies the signal to noise ratio is better using the fibre to image the aperture, which we attribute to the fact the fibre can be in closer contact to the aperture than the antenna chip by itself, yielding higher overall power at the antenna. Good agreement with experiment is observed, considering the detrimental impact of noise for signals at lower frequencies.

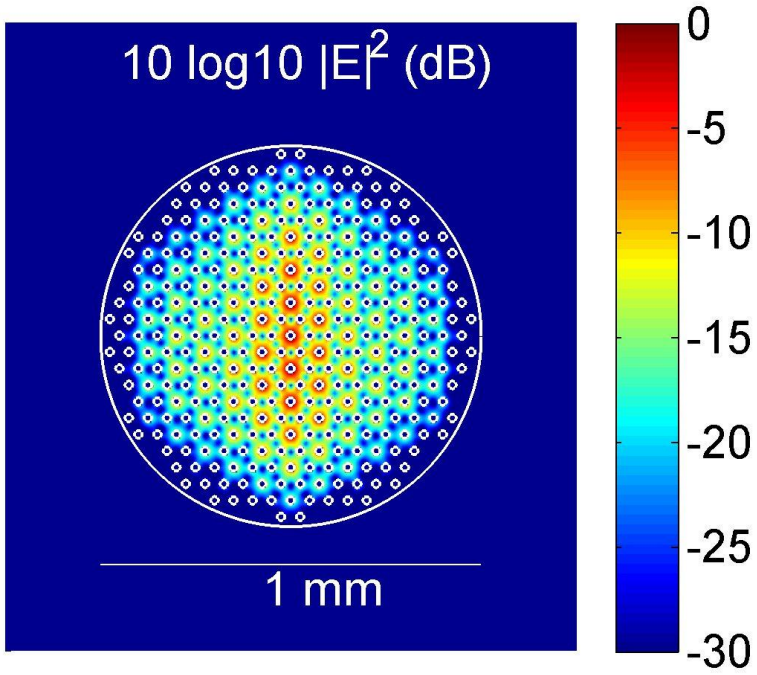

Supplementary Figure S4: Schematic of the two-dimensional simulation space. Our model considers a 1 mm-diameter circular fibre with hexagonally arranged circular wires of 20 μm diameter and with 50 μm centre-to-centre pitch. The optical properties of Zeonex and indium are accounted for[29,31]. This illustrative example of confined wire modes shows the field intensity on a logarithmic colour scale, calculated for the metamaterial fibre at a frequency of 0.1 THz, possessing an effective index of $n_{\text{eff}} = 1.538 + 0.020i$.

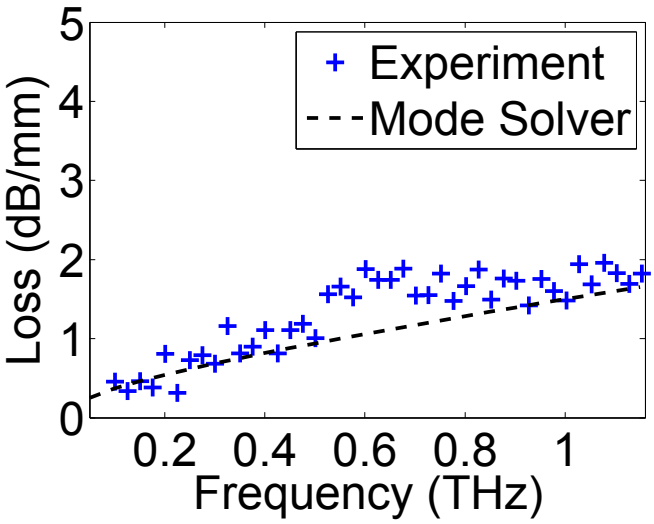

Supplementary Figure S 5: Fibre loss. Measured and calculated loss (straight fibre section), as described in the Methods section. Note that the 95% confidence interval for the loss coefficient yields very large errorbars (not shown), of the order of $\pm 1\,\mathrm{dB/mm}$. This is inevitable, considering that only three relatively noisy data points are considered for the linear fit. Additionally, Fabry-Perot resonances are expected to induce frequency-dependent fluctuations in intensity, that are dependent on the slab length. More measurements with longer samples would of course result in smaller errorbars. This data should thus be interpreted as an estimate. Loss is also calculated from the two-dimensional finite-element mode-solver presented as discussed in the Methods section. A comparison between experiment and simulation shows satisfactory agreement. This suggests that the small imperfections in the wire array — both in the axial direction, and in the cross-section [Fig.1(e)-(g)] — do not noticeably deteriorate the transmission properties of the fibres.

Supplementary Reference

[32] Genet, C. & Ebbesen, T.W. Light in tiny holes. *Nature* **445**, 39-46 (2007).